Coastal Dynamics 2017
Paper No. 094

SEDIMENT EROSION IN ZERO-MEAN-SHEAR TURBULENCE

Marie Rastello[1], Hervé Michallet[1] and Jean-Louis Marié[2]

Abstract

A stirring grid, in a square tank, located more than 2 mesh sizes away from a sediment layer, is used to study particle erosion by a zero-mean-shear turbulence. The particle concentration has been monitored using an OBS technique and fluid velocity mostly through PIV. Particle lift-off and concentration in the tank are shown to rise sharply as the grid frequency is increased. Converged velocity profiles indicate that the bulk isotropy of the turbulent velocity in the tank, well predicted by a slightly modified Matsunaga et al. (1999) model, gets broken close to the bed. While mean shear rates are shown to be small at the bed surface, some high shear level events induced by vortex impacts are assumed to be responsible for the particle erosion.

Key words: bed erosion, diffusive turbulence, stirring grid, zero-mean-shear turbulence

1. Introduction

Sediment erosion and transport are ubiquitous in nature in general (in rivers, snow avalanches, turbidity currents, snow/sand transport by the wind, etc.) and in the coastal environment in particular (beach erosion, sink holes, underwater sand transport…). Since the pioneering work of Shields (1936), it is common to think that erosion takes place when bed shear stress reaches a critical threshold that triggers incipient sediment motion and suspension. This critical threshold is generally related to mean flow properties. However, it hardly accounts for the non-uniform, non-stationary, intermittent or turbulent character of many natural flows. For a long time, the presence of coherent vortex structures and/or strong turbulent events near the bed have been suspected to play a significant role on bed erosion. A number of studies in channel-flows attest this idea (Kaftori et al., 1995, Nino et al., 1996, Vincovic et al., 2011). However, as these flows are not free of mean shear, the influence of turbulence alone on sediment transport is still under debate. The objective of this research is to investigate sediment/turbulence interaction in connection with erosion under zero-mean shear flow. One way to experimentally do that is to use the diffusive turbulence produced by an oscillating grid (Yan et al., 2007). The study of the flow produced by an oscillating grid without sediments (Hopfinger and Toly, 1976, De Silva and Fernando, 1994, Matsunaga et al., 1999) showed that far enough from the grid, the mean flow is weak while turbulence appears to be homogeneous and almost isotropic. Indeed, a careful design of the grid helps to inhibit mean secondary flows (Fernando and De Silva, 1993). This oscillating-grid turbulence (OGT) has been used by various authors in the past to investigate different aspects of sediment suspension. When the grid is located close to the bed of sediment it mimics the action of fluctuating stresses acting on this bed. Huppert et al. (1995) and Gratiot et al. (2005) adopted this location to study steady suspensions properties such as highly concentrated suspensions and lutocline formation. Very recently Traugott et al. (2017) used a high solidity grid set up farther from the particle layer to investigate the forces involved in the lift-off of particles into turbulent flow, from 3D-PTV tracking of particle motion. In this experiment, we use an oscillating grid placed more than 2 mesh sizes above the bottom of the tank, as Tsai and Lick (1986) did. Optical Backscatter Sensors (OBS) and Particle Image Velocimetry (PIV) are used to characterize the flow within the tank and especially close to the sediment layer, the amount of particles set in suspension by the generated turbulence and how both are

[1]Univ. Grenoble Alpes, CNRS, Grenoble INP, *LEGI,* F-38000 Grenoble, marie.rastello@legi.cnrs.fr, herve.michallet@legi.cnrs.fr
[2]Univ. Lyon, CNRS, *LMFA,* F-69000 Ecully, jean-louis.marie@ec-lyon.fr

related. The paper is built as follows. After presenting the experimental device and the measuring techniques we have used (§2), we draw our attention to the concentration of sediment that is obtained when the grid is oscillating and a sediment bed is present at the bottom of the tank. Transient and final states are addressed (§3). Velocity measurements and erosion processes are then investigated with a special attention to their coupling (§4).

2. Experimental device and measurements

2.1. *Experimental device*

A Perspex tank (53 cm × 53 cm × 90 cm) is filled with a glycerin/water mixture (density: ρ_f = 1157 g/L, viscosity: $\nu = 10.8 \times 10^{-6}\ m^2 s^{-1}$) up to h = 40 cm (see figure 1). A 2 cm bed of plastic particles (density: ρ_s = 1180 g/L, size: d_{50} = 0.450 mm, settling velocity: w_s = 0.2 mm/s) is setup through deposition at the bottom of the tank. A stirring grid (mesh size: M = 7.5 cm, bar width: m = 1.5 cm, stroke S = 4.5 cm) is fixed on a central vertical moving axis at a 20 cm mid-position above the bed. The axis is set in motion by a motor with a horizontal axis entraining an eccentric device that converts it to the expected vertical oscillating one (Gratiot, 2000). One run corresponds to an oscillation frequency f < 6 Hz for the grid. Minimum duration of a run is 10 minutes (velocity measurements), maximum one is up to 60 hours (concentration measurements). Part of the runs were performed with fluid only in the tank, the others were with fluid + particles. A glycerin/water mixture was preferred to a water only experiment to have a density ratio more favorable to particles' lift-off by the turbulence reaching the bed. One density for the mixture has been explored so far, some others will be as well in the future.

2.2. *Measuring features*

When dealing with fluid + particles experiments, long runs were performed (up to 60 hours) and particle concentration evolution was monitored using two different techniques (see figure 1). Two optical backscatter sensors (OBS-3+/Campbell Scientific) located one just below the lower position of the grid and the other 10cm above the first one were used to monitor concentration evolution in the tank through time. The acquisition rate was 4 Hz. Sampling at the height of the lower OBS was performed as well so as to provide a calibration curve for the OBS. One to two liters of particles + fluid were pumped out of the tank at once during the run using a peristaltic pump. Filtration of the particles followed by a careful drying in a drying chamber was performed. Weight measurement was then performed with a scale. Two types of velocity measurements were done. A Nortek-ADV Vectrino was used to measure the fluid velocity from 0.5cm up to about 10cm above the bottom of the tank in fluid only configurations. The sensor was held from above by a rod and immersed in the tank below the grid. The sensor was side-looking, i.e. measuring velocities on some points farther horizontally from its position.

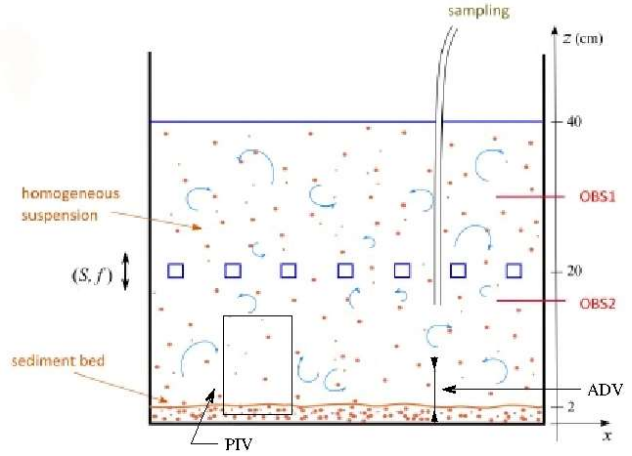

Figure 1. Sketch of the experimental measuring device

PIV measurements have been performed using a laser (2 × 200mJ, 532 nm) and polyamide round Dantec particles (size: 20 µm, density: 1.03 kg/m^3) together with silver coated Dantec spherical glass particles (size: 10 µm, density: 1.4 kg/m^3) as tracers, depending on the run. The choice of PIV tracers turned to have no influence on the results of the measurements. Images were taken with an Imager Pro X2M / LaVision camera with an acquisition rate of 29 fps. Different field sizes were explored: FS1 (14 cm × 10.5 cm, resolution: 0.1 cm), FS2 (4.7 cm × 3.5 cm, resolution: 0.3 mm), FS3 (2.4 cm × 1.8 cm, resolution: 0.1 mm). Some runs were done with fluid only, the others with fluid + particles. All the images were including either the bottom of the tank or the upper layers of the particle layer when present (see figure 1). Typical PIV runs lasted 10 minutes.

3. Concentration measurements

During each run, the particle concentration evolves in time, but stays spatially homogeneous in the tank. This was validated by the two OBS located 10 cm apart that indicate the same concentration. As a consequence, sampling was done in one position only and was used to establish the OBS calibration curve (output voltage versus concentration). The calibration curve obtained by comparing OBS results with sampling ones is accurate when concentration is greater than $2 \times 10^{-1}\,\mathrm{kg/m^3}$. Below this value a discrepancy up to a factor 2 appears in the results. It is taken into account by adding error bars in Figure 3. Once properly calibrated against weighted samples, the OBS were used to measure the evolution of the average sediment concentration C during long time runs. This sediment concentration results from a balance between the settling flux within the whole tank (depth h) and the erosion flux at the sediment bed F_e:

$$\boldsymbol{h\frac{dC}{dt} = F_e - w_s C} \qquad (1)$$

This first order differential equation has the following solution:

$$\mathbf{C = (C_0 - C_f)\,exp\left(-\frac{w_S}{h}t\right) + C_f} \qquad (2)$$

where C_0 is the initial concentration and C_f the concentration at equilibrium when settling and erosion flux fully balance ($F_e = w_S C_f$). From time variation of C, it is thus possible to estimate the settling velocity and flux for a given oscillating frequency of the grid. This is achieved by calculating w_S , C_f that provide the best fit of the experimental data with (2). The reliable estimation of these parameters often requires measurements over more than 5 hours. An example showing the time variation of C obtained for a long run is presented in figure 2. The run is composed of successive time sequences with various stirring frequencies of the grid between 0 and 6 Hz. Sequences were recorded continuously one frequency being set directly after the previous one. Frequencies and sequence durations were adapted at best to fulfil practical constraints in the lab. As a result, the sequences duration differ from one run to another one. We distinguish in figure 2 erosion sequences, so called when the run begins from a state in which all the particles are deposited at the bottom of the tank, from sedimentation sequences, when the run begins with all the sediments previously set up in suspension manually. The exponential fit for each sequence is plotted in the figure. We note that third and fourth sequences correspond to the same stirring frequency, but are fitted with two different exponential functions. This is explained by the fact that the particles size of the sediment is not uniform, implying a sorting of the particles with time. It means that smaller particles are eroded before the larger ones, which manifests in slightly different erosion flux. Same behavior applies to sedimentation cases, where a similar sorting within the suspension is also expected. Final concentration, settling velocity and fluxes were estimated in this way from seven acquisitions covering a total of about 900 hours, including 200 hours of grid action. These data are plotted in figure 3. Results for low frequencies (f < 3Hz) are likely less reliable, corresponding to very low concentrations for which the calibration curve exhibits a significant scatter. As expected and observed experimentally, increasing the oscillation frequency of the grid increases the amount of particle eroded and set in suspension. Indeed, as it is well known (Hopfinger and Toly, 1976, Matsunaga et al., 1999) and validated in §4, increasing the

oscillation frequency increases the flow rates and turbulent levels even far from the grid. Turbulence being more energetic close to the bed and in the bulk, increasing oscillation frequency may also imply bigger particles to be set and maintained in suspension as well. This would correspond to the increase in settling velocity of the particles with *f* that can be seen in figure 3 (up-right). Erosion flux being a combination of both concentration and settling velocity follows with an increase as well.

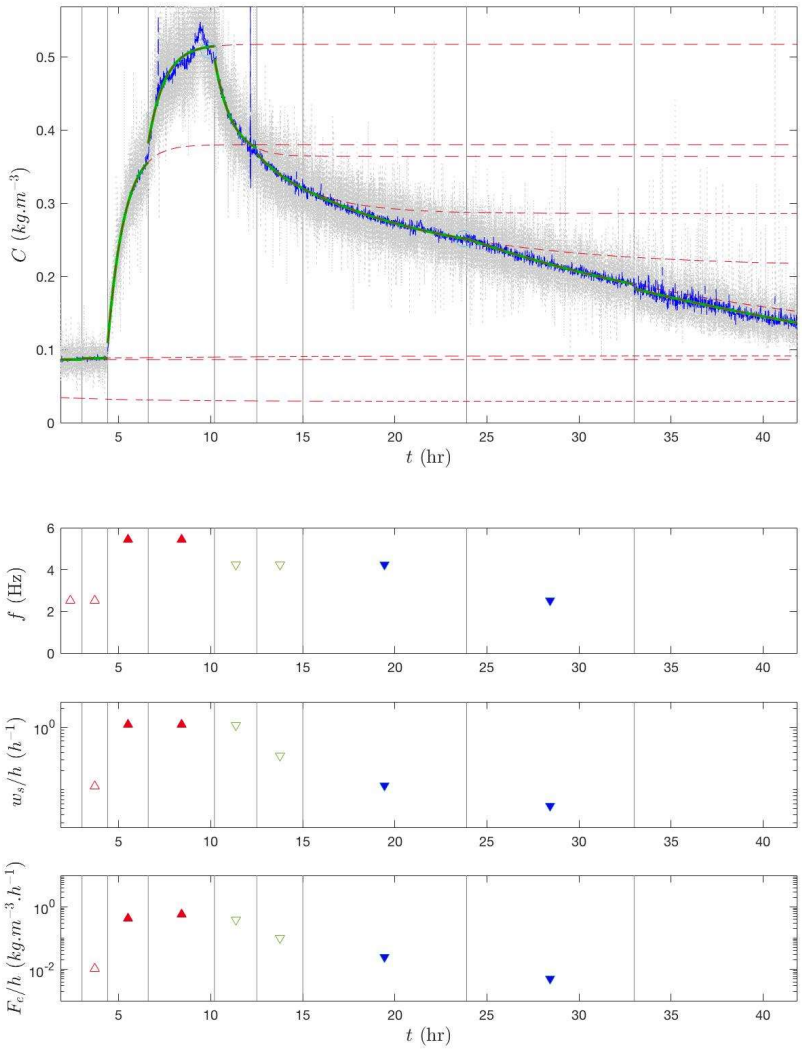

Figure 2. Upper part: time variation of concentration along with exponential fittings for different grid oscillating frequencies and particle sorting. Dashed black line: measured concentration with a 4Hz acquisition rate, blue line: sliding average of the measured values on a 25s basis, red dashed curves: exponential fittings. Bottom part: corresponding frequencies, settling velocities and erosion fluxes both divided by the depth of the fluid. Upward red (downward blue) triangles correspond to erosion (deposition) cases. Empty symbols are for a duration too short to be taken into account: less than 2 hours for erosion, less than 4 for deposition.

A point that is worth to notice is that whatever the initial conditions (settled bed or all the particles

previously suspended), the so called erosion and deposition sequences end in the same results indicating that there is no hysteresis driving both erosion fluxes and concentration in the tank. The plateau that can be seen for low frequencies has probably not enough points in any of the 3 graphs to assess as a fact that before the increasing tendency there is a constant phase. Nevertheless, these data suggest that first at low frequencies the turbulent flow close to the bed is not able to erode any particles (f ≤ 2Hz), then it is able to erode very fine particles only (d # 0.350 mm, w_s # 6 × $10^{-5} m.s^{-1}$) and erosion and concentration are not depending directly on the frequency value in this range of parameters. With a further increase in grid frequency and levels in turbulence, more and more numerous and larger particles are eroded up to all fractions in the bed (d_{50} # 0.450mm, w_s = 0.2 mm/s). Erosion and bulk concentration are then directly increasing with grid oscillation frequency. For the larger frequencies (f > 4Hz) a tendency appears that scales in f^5 for the final concentration, f^{10} for settling velocity and f^{15} for erosion flux. At that stage the interest of these fittings do not rely on the value of the exponents themselves, whose physical meaning is not clear but in the fact that they are consistent with $F_e = C_f w_s$. The scatter around the main tendency being less important for the erosion flux than for the final concentration indicate that the particle sorting that can be observed during long runs is only a side effect when considering the erosion flux in the tank at a given frequency.

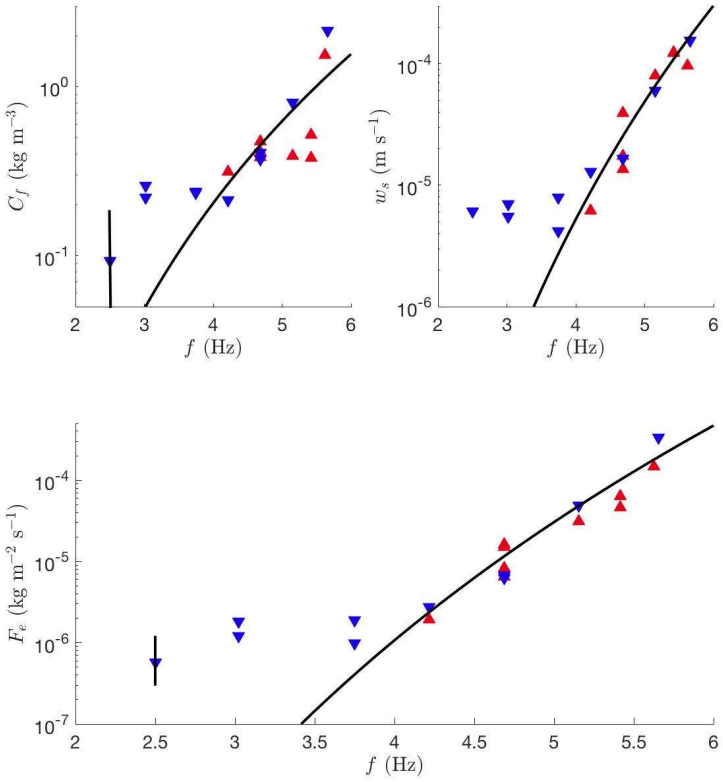

Figure 3. Log versus linear graphs. Up-left: concentration at equilibrium versus frequency, black curve: $\mathbf{2 * 10^{-4} * f^5}$. Up-right: settling velocity versus frequency, black curve: $\mathbf{5 * 10^{-12} * f^{10}}$. Bottom: Erosion flux versus frequency, black curve: $\mathbf{10^{-15} * f^{15}}$. Upward red (downward blue) triangles correspond to erosion (deposition) cases. Black error bars are taking into account OBS calibration discrepancy for very low concentrations ($\mathbf{C < 2 \times 10^{-1}\ kg/m^3}$).

4. Velocity measurements and erosion process

4.1. ADV/PIV velocity measurements

As mentioned before two types of velocity measurements have been performed. First, a short ADV campaign was led. The measurements exhibited some qualitatively interesting and coherent results. More than 2 mesh sizes away from the grid, whatever our stirring frequency, mean velocities were shown to be lower by about an order of magnitude than fluctuating ones. The turbulence in this region was shown to be mostly isotropic. Indeed, both horizontal velocities exhibit the same values while vertical one remains a little bit larger as it is usually the case in this kind of experiments (De Silva and Fernando, 1994). When we get in the region by the bed, isotropy breaks and vertical fluctuating velocity goes low more rapidly than horizontal one does, both reaching zero at the bed location. Because the sensor was fixed on a rod passing through a mesh of the grid, it was very difficult to prevent the whole device from vibrating. Biases to the measurements linked to this vibration together with the ones that can come up from the physical presence of the sensor immersed in the fluid incited us not to reach in for some more quantitative results at that stage. A more extensive campaign was done using PIV, taking advantage of the fact that no sensor had to be immersed below the grid with that measuring technique (no sensor vibration, no flow disturbance…). First point comes with validation of the measurement. Examples of statistical convergence are presented in figure 4, together with power spectral density in figure 5.

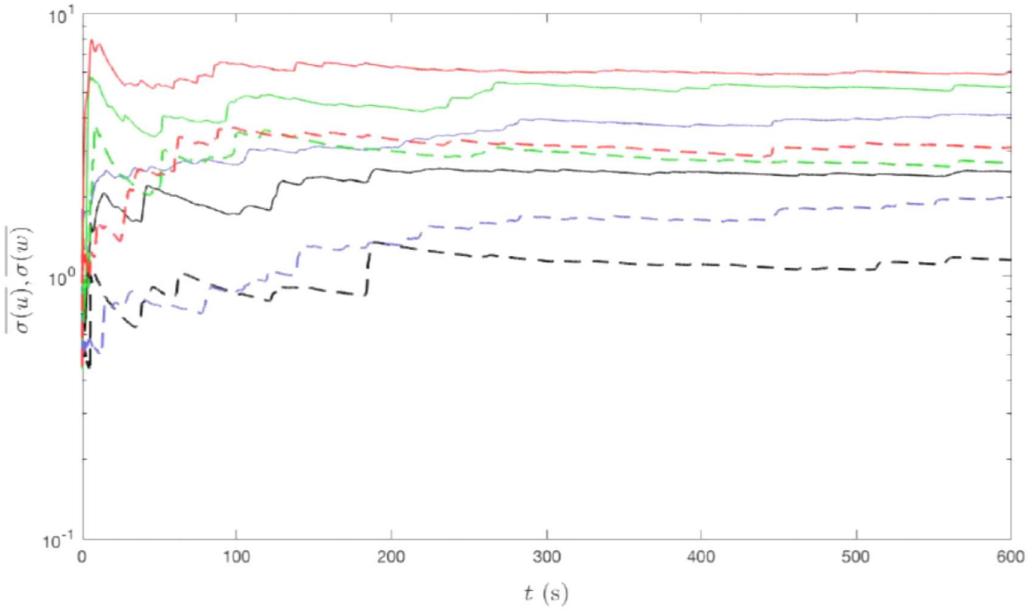

Figure 4. Black: f = 3 Hz, blue: f = 3.7 Hz, green: f = 4.7 Hz, red: f = 5.6 Hz, full lines: horizontal velocity (u), dashed lines: vertical velocity (w). Convergence of the standard deviation of the velocities $\boldsymbol{\sigma(v = u, w) = \sqrt{\sum_0^t (v - \overline{v})^2 / t}}$ versus time. Field of view used for this figure is FS1.

As can be seen in figure 4, the sampling/recording process is adapted to obtain variables (velocities and shear) that are converged. The spectra in figure 5 have different interesting features. Among the noise at high frequencies the oscillating frequency of the grid appears. This is likely due to a light shaking of the whole tank due to some vibrations transmitted by the motor, that we were not able to completely get rid of. Nevertheless, these peaks are very localized and represent little energy, immersed in the noise region (f > 1 Hz) and do not seem to influence the energy cascade. The expected energy cascade is present for both horizontal and vertical velocities. The slopes of the decreases can be approximated by a -5/3 slope over roughly one decade but the evolution of these spectra with grid frequency has not yet been analyzed in

details. The plateau on the left side of the spectra shows the existence of some energetic large scale turbulent eddies. They are one of the key parameter of the erosion process that will be tackled in the next part. Turbulent velocity profiles are

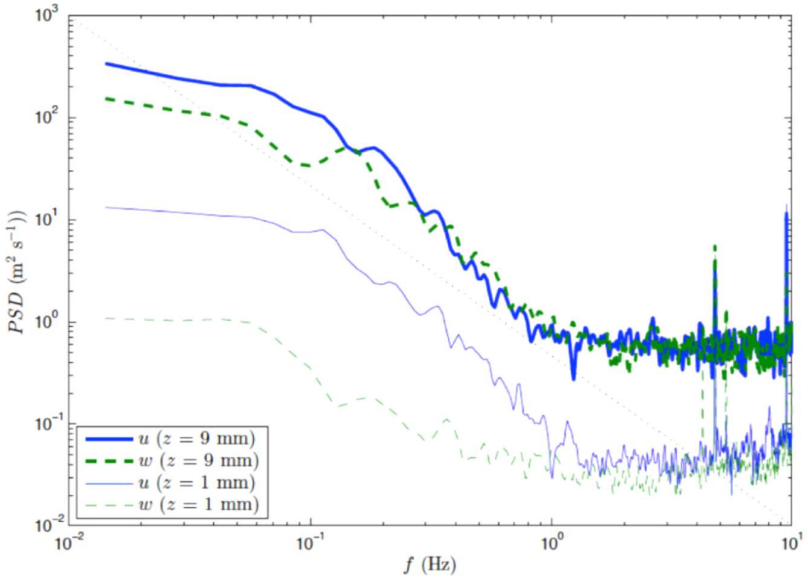

Figure 5. Power spectral density versus frequency, dashed black line: slope -5/3. Field of view used for this figure is FS1. Grid oscillation frequency: f=4.7Hz.

presented in figure 6 (top-left). They correspond to one of our large field of view (FS1) and hence give a wider glance at what is occurring in the tank. Smaller fields of view will be used when dealing with eroding processes directly. The qualitative features that had been observed with the ADV are here confirmed quantitatively. In the region less than 2 mesh sizes away from the grid (z > 5 cm), the turbulence is not isotropic with a predominance of the vertical velocity, together with mean flow velocities (not presented in the graph for clarity's sake) that are not negligible, as previous studies have mentioned (see Atkinson et al., 1987 for example). More than 2 mesh sizes away (z < 5 cm) turbulent velocity appears to be isotropic and mean velocity to be of second order values. From the profiles one can see that this established isotropy is then broken by the presence of the bed (z < 2 cm) which effects are first to increase the horizontal velocity while decreasing the vertical one then followed by a rapid decrease to zero of both of them when reaching the bed location. Turbulent kinetic energy on its side is well approximated by a slightly modified Matsunaga et al. (1999) predictive model until bed vicinity is felt by the flow. Indeed, while collapsing all the gathered data the authors chose to fit the $\boldsymbol{k_0}$ to *Re* dependency by a set made of a constant, for *Re* numbers larger than $\mathbf{5.5 \times 10^3}$ and by a dependency in $\boldsymbol{Re^{1/2}}$ for *Re* numbers lower than $\mathbf{5.5 \times 10^3}$. Of course, even if collapsing pretty well, the data are a little bit spread and different empirical relations can be drawn from them. Keeping the same format as Matsunaga et al. (1999) we only modified the exponent in the variable part of the tendency from a $\boldsymbol{Re^{1/2}}$ to a $\boldsymbol{Re^{0.47}}$ which fits as well as the authors' relationship to the gathered data and give a way better correlation with our own results. The fact that Matsunaga et al (1999)'s conclusions were mostly drawn out of experiments with a $\boldsymbol{S/M}$ value of 0.8 while we are working with a ratio of 0.6 is probably one key that can explain this small discrepancy in the model to be used to predict the data. As mentioned before, when getting close to the bed, modified or non-modified Matsunaga et al. (1999)'s model will then overestimate the turbulent kinetic energy since bed presence is making it decrease to zero more rapidly than the bulk normal decrease. Shear rate figure (figure 6 – bottom) points on very interesting features. As expected, as we get farther from the grid, shear rate coming from the mean flow vanishes and the flow that reaches the bed in this experimental configuration can definitely be considered as a zero-mean shear one. This point will be of high importance when dealing with the eroding part topic (next section). The averaged turbulent shear rate does not exhibit specifically high values as well. Besides these small values, another important feature comes from the maximum shear

rate measured, which on its side is approximately 10 times larger than the averaged values. These maximum values are linked to some very energetic structures that build up and travel in the tank from the grid reaching at some point the bottom of the tank. From what we observe experimentally they are the ones responsible for the particles' erosion from the sediment bed.

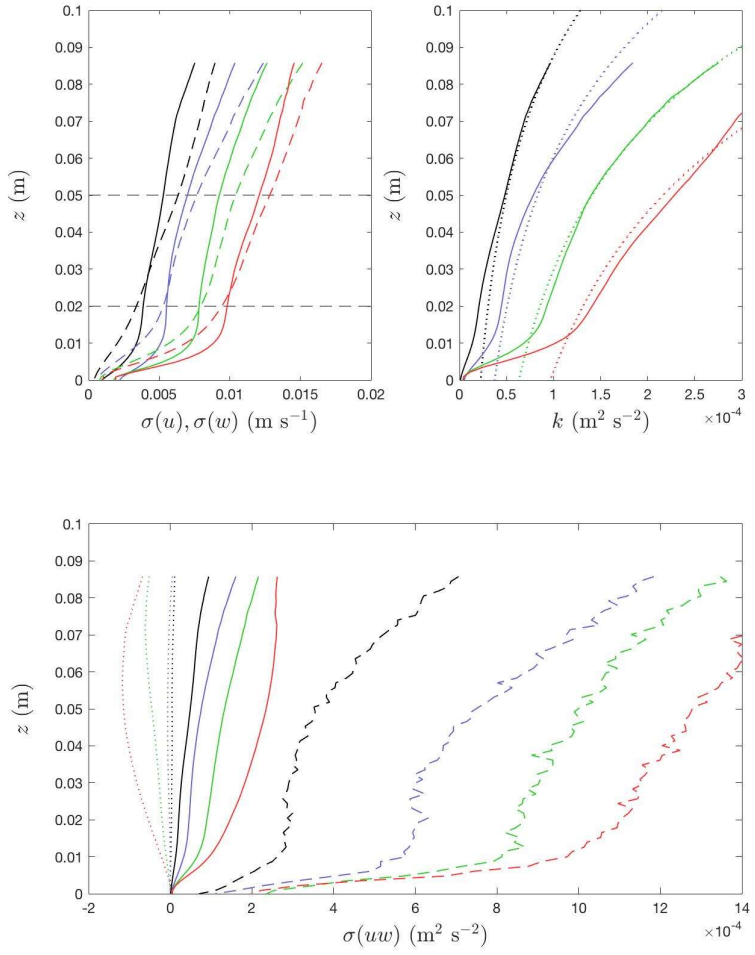

Figure 6. Black: f = 3 Hz, blue: f = 3.7 Hz, green: f = 4.7 Hz, red: f = 5.6 Hz. Top/left: fluctuating velocity profiles, plain lines: σ(u), dashed lines: $\boldsymbol{\sigma(w)}$. Dashed horizontal lines are here to materialize the zone (between the 2 lines) in which isotropy exists. Top/right: Turbulent energy profiles, plain line: experimental values, dotted lines: Matsunaga et al. (1999) modified model predictions. Bottom: shear profiles, plain lines: turbulent shear $\boldsymbol{\sigma(uw)}$, dotted: mean shear $\overline{\boldsymbol{uw}}$, dashed lines: maximum shear. Field of view is FS1.

4.2. Bed erosion by a zero mean shear turbulence

Particle's erosion is usually linked to mean shear flow that, when getting large enough, is able to set sediments in motion through either bed load or suspension. The occurrence of the erosion, in that case, is governed by the Shields parameter that compares the mean shear flow at the surface of the sediment layer

with the relative weight of the sediment (Shields, 1936). When the Shields number exceeds a critical value, particles from the bed can be set in motion. More recently, interest was drawn to other ways of mobilizing sediments. Among them, the impact of a vortex ring with a sediment bed has been studied together with the sediment mobility linked to it (Munro et al., 2009, Bethke et al., 2012). The authors of the study observed that when the vortex ring is reaching the bed vicinity it gets deformed, growing horizontally and shrinking in the vertical direction. This geometrical modification gives rise to an enhancement of the horizontal velocity and a reducing of the vertical one. Together with this deformation a small region with an opposite vorticity gets created at the edge of the main vortex. As the vortex gets closer, the along-bed velocity of the fluid increases, generating some local shear stress that sets the particles in motion towards the side of the vortex. At the edge of the vortex, the horizontally moving particles are then set up in suspension at first along the streamline that goes all around the primary vortex. A kind of Shields parameter is built using the relative weight of the particles together with a local shear stress evaluated from the local quantities that set the particles in motion such as local bed velocity when measured and if not available the vortex travelling velocity with the assumption that the bed one is directly related to it. In the present experiment, as mentioned before, there is no mean shear at the bed surface, which suggests that another mechanism is involved in bed's mobilization

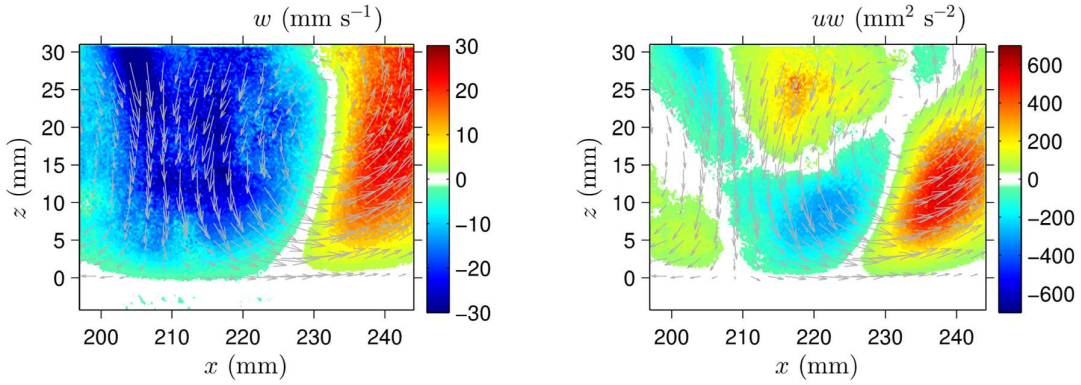

Figure 7. Downward traveling structure generating high shear rates at the sediment layer (medium field of view – FS2).

The turbulent flow generated by the grid diffuses downward and impacts the sediment layer. Since turbulence can be seen, in some ways, as a superposition of vortices of different sizes and strengths, one possible scenario could be that some vortices are not powerful enough to set the particles from the bed in motion and some others, with more strength, are able to generate a local shear at the bed location that is above the one which is needed to set the particles in suspension. PIV velocity fields gave us the opportunity to visualize some of these structures that could be assimilated to traveling vortices, generating high levels of shear at the bed's location. An example of it is in figure 7. As a side result, some of the PIV experiments with a sediment layer enabled us to track the eroded particles while they were getting set in suspension by the flow. This happened to be a good way to spot the phenomena that could be involved in picking up the particles from the layer. The only problem was that, to have particles covering enough pixels to be detected, we had to track them only on the small fields (FS3) which was great for having a more precise determination of velocities and shear stresses but was enabling us to see only a 2 cm region of the bed during the run and hence reducing the probability to have eroding events happening in that portion of the tank during a run. Nevertheless, we did get to spot some particles lifted from the bed and to check on the flow characteristics at that moment but not in a sufficient amount to be able to make statistics out of them. One example of a shear + vertical velocity map can be seen in figure 8 together with some particle departures' prints. On this figure eight particle's departure from the sediment layer have been detected. At least seven of them have happened in a region in which shear was rather large and vertical velocity was positive indicating that both quantities were in favor of a picking up by some structure that was exhibiting a high shear value and positive vertical onset. Some work is still on on that topic to be able to transform this qualitative statement in a more quantitative one but the smallness of the field and the lack of contrast on the PIV images due to the presence of the particles are making it quite challenging.

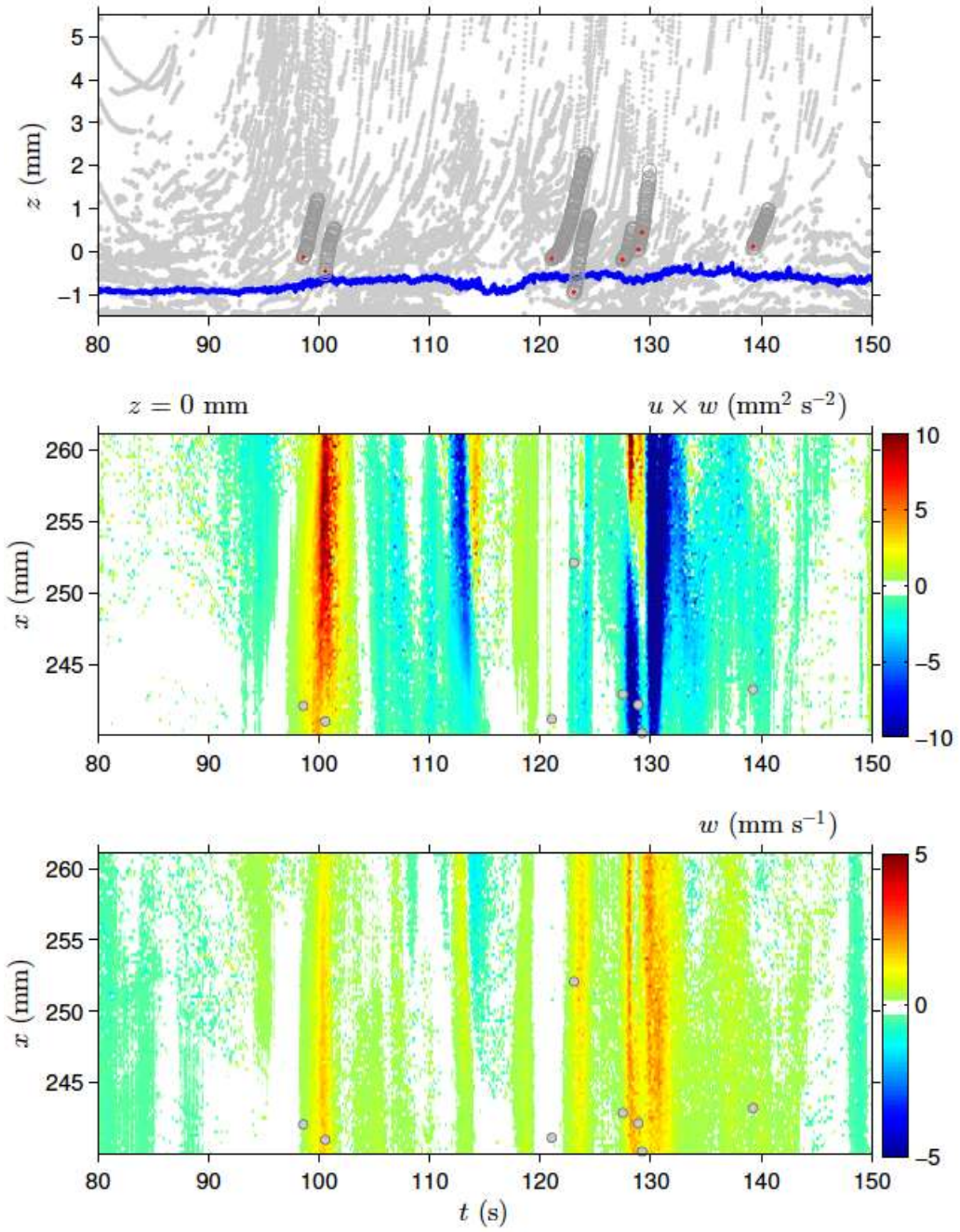

Figure 8. Maps versus time. Top: Vertical positions in the field, all x positions are gathered on one corresponding point. Blue line: sediment layer height, grey dots: sediment particles detected, red dots: initial position of a particle eroded from the sediment layer and tracked afterwards. Dark grey circles: position of the particles coming from a red dot. Middle: instantaneous shear stresses are mapped on a t-x map at the height z=0. Bottom: instantaneous vertical velocities are mapped on a t-x map at the height z=0. Field of view is FS3.

Conclusion

A stirring grid experiment was used to study the erosion of particles from a sediment layer, in the absence

of mean flow at the bed location. Varying the stirring frequency and thus the energy input in the tank the concentration of particles was monitored in the tank, showing a net increase of the particles set up in suspension as the frequency is increased. Velocity measurements have shown that more than 2 mesh sizes away from the grid, the turbulence is homogeneous and quasi-isotropic as most of the previous studies have already mentioned it and can be modeled by a modified-Matsunaga et al. (1999)'s model. As bed is approached, isotropy breaks and both velocities (horizontal and vertical) go to zero but with the vertical one going more rapidly than the horizontal one that begins at first by increasing. First hints on the erosion process have been obtained with PTV and PIV by observing some particle lift–off in connection with the turbulent flow field at the bed surface. They give a first insight on the mechanism involved in erosion in a flow free of mean shear. They suggest that, while weaker vortices are not able to set particles in suspension, the ones that are having a greater energy are able to lift particles and generate a suspension of particles.

Acknowledgements
The help of L. Vignal for video capturing and PIV pre-processing is gratefully acknowledged. M. Bezhadi participated on preliminary concentration measurements. S. Mercier and S. Pioz contributed to improve the grid mechanical stirring.

References

Atkinson J.F., Damiani L., and Harleman D.R.F., 1987. A comparison of velocity measurements using a laser anemometer and a hot-film probe, with application to grid-stirring entrainment experiments, *Phys. Fluids*, 30, 3290.

Bethke, N., & Dalziel, S. B., 2012. Resuspension onset and crater erosion by a vortex ring interacting with a particle layer. *Phys. Fluids*, *24*(6), 063301.

De Silva, I. P. D., and Fernando H.J.S., 1994. Oscillating grids as a source of nearly isotropic turbulence. *Phys. Fluids* 6.7: 2455-2464.

Fernando H.J.S. and De Silva I.P.D., 1993, Note on secondary flows in oscillating-grid, mixing-box experiments. *Phys. Fluids* **5**(7), 1849–1851.

Gratiot, N., 2000, Etude expérimentale de la formation des couches de crème de vase turbulentes, *phd thesis, Univ. J. Fourier, Grenoble.*

Gratiot, N., Michallet, H. and Mory, M., 2005. On the determination of the settling flux of cohesive sediments in a turbulent fluid. *Journal of Geophysical Research: Oceans*, *110*(C6).

Hopfinger, E. J., and Toly J.A., 1976. Spatially decaying turbulence and its relation to mixing across density interfaces. *J. Fluid Mech.* 78(01): 155-175.

Huppert, H. E., Turner J.S. and Hallworth M.A., 1995. Sedimentation and entrainment in dense layers of suspended particles stirred by an oscillating grid. *J. Fluid Mech.* 289: 263-293.

Kaftori, D., Hetsroni, G., and Banerjee, S. Particle behaviour in the turbulent boundary layer. I. Motion, deposition, and entrainment. *Phys. Fluids* **7**, 1095–1106 (1995).

Matsunaga, N., Sugihara, Y., Komatsu, T. and Masuda, A., 1999. Quantitative properties of oscillating-grid turbulence in a homogeneous fluid. *Fluid dynamics research*, *25*(3) : 147-165.

Munro, R.J., Bethke, N. and Dalziel, S.B., 2009. Sediment resuspension and erosion by vortex rings. *Phys. Fluids (1994-present)*, *21*(4), p.046601.

Niño, Y., García, M., 1996. Experiments on particle-turbulence interactions in the near wall region of an open channel flow: implications for sediment transport. *J. Fluid Mech*. 326, 285–319.

Shields, A., 1936. Application of similarity principles and turbulence research to bed-load movement. *Soil Conservation Service*.

Traugott, H., Liberzon, A., 2017. Experimental study of forces on freely moving spherical particles during resuspension into turbulent flow. *Int. J Multiphase Flow* 88,167–178.

Tsai, C.H. and Lick, W.,1986. A portable device for measuring sediment resuspension. *Journal of Great Lakes Research,* 12, 314-321.

Vinkovic, I., Doppler, D., Lelouvetel, J., Buffat, M., 2011. Direct numerical simulation of particle interaction with ejections in turbulent channel flows. *Int J. Multiphase Flow,* 37 ,187–197.

Yan, J., Cheng, N.S., Tang H.-W., Tan S.K., 2007, Oscillating-grid turbulence and its applications: a review. *J. Hydr. Research*, 45 (1), 26-32.